ARTICLE

Light harvesting indolyl-substituted phosphoramide ligand for the enhancement of Mn(II) luminescence

Received 00th January 20xx,
Accepted 00th January 20xx

DOI: 10.1039/x0xx00000x

Marco Bortoluzzi,*[a,b] Jesús Castro,*[c] Alberto Gobbo,[d] Valentina Ferraro [a] and Luca Pietrobon [a]

The reaction of *N*,*N*,*N*',*N*'-tetramethyl-*P*-indol-1-ylphosphonic diamide (L) with Mn(II) halides under mild conditions allowed the isolation of tetrahedral neutral complexes having general formula $[MnX_2L_2]$ (X = Cl, Br, I). The structures of the new coordination compounds were ascertained by single-crystal X-ray diffraction. The three species exhibited noticeable luminescence in the green region upon excitation with UV light, with emissions related to the Mn(II) $^4T_1(^4G)\rightarrow{}^6A_1(^6S)$ transition, without appreciable luminescence from the coordinated ligands. Luminescence was caused by both metal and ligand excitations. The good light harvesting features of the indol-1-yl fragment allowed the luminescence enhancement with respect to comparable phenyl-substituted derivatives.

Introduction

Ligands containing the [O=P]-donor moiety are of paramount importance for the preparation of Mn(II) luminescent coordination compounds. The first example was the tetrahedral triphenylphosphine oxide complex $[MnBr_2(O{=}PPh_3)_2]$, described for the first time in 1961 by Cotton and co-workers.[1] The species is of actual interest because of its triboluminescent and ferroelectric features.[2] Recently, bidentate phosphine oxides were employed for the preparation of luminescent derivatives with coordination numbers ranging from four to six. Noticeable examples are green-emitting tetrahedral halide complexes with bis[2-(diphenylphosphino)-phenyl]ether dioxide behaving as chelating ligand.[3] The structurally similar 4,6-bis(diphenylphosphino)dibenzofuran dioxide was used to synthesize tetrahedral chloro- and bromo-complexes, the last one successfully applied for OLED fabrication.[4] Tetrahedral derivatives were also isolated from the reaction of $MnBr_2$ with 1,2-bis(diphenylphosphino)ethane dioxide ($dppeO_2$), with the ligand acting as bridge between two Mn(II) centres. The coordination polymer $[MnBr_2(dppeO_2)]_n$ exhibited luminescence vapochromism related to the reversible coordination of dimethylformamide, with formation of trigonal bipyramidal Mn(II) centres.[5] An octahedral homoleptic complex with κ^2-$dppeO_2$ was also reported, and an analogous species was obtained using bis(diphenylphoshino)methane dioxide ($dppmO_2$).[5,6] Organic–inorganic hybrid complexes $[Mn(L)_3][MnX_4]$ (X = Cl, Br) characterized by thermochromic behaviour were synthesized by reacting $MnCl_2$ or $MnBr_2$ with bis(phosphine oxide) ligands such as $dppmO_2$, $dppeO_2$ and 2,3-bis(diphenylphosphino)-1,3-butadiene dioxide ($dppbO_2$).[7] The comparable $[Mn(dppbO_2)_3][Mn(NCS)_4]$ species was isolated starting from $Mn(NCS)_2$, and further octahedral Mn(II) luminescent complexes with mixed coordination sphere were obtained using bis(diphenylphosphino)ethane dioxide and 3,4-bis(diphenylphosphino)isobutene dioxide.[8] These last compounds exhibited excitation-tuneable dual luminescence derived from intraligand fluorescence and Mn(II)-centred phosphorescence. Octahedral Mn(II) was also observed in the coordination polymer synthesized from the reaction of 1,2,4,5-tetrakis(diphenylphosphino)benzene tetraoxide with $Mn(ClO_4)_2{\cdot}6H_2O$ in dimethylformamide.[9] The use of *N*,*N*-dimethylamino)bis(diphenylphosphino)methane dioxide as ligand L allowed the isolation of the cationic complexes $[MnClL_2]^+$ and $[MnBrL_2]^+$, first examples of luminescent Mn(II) derivatives with square-pyramidal (C_{4v}) geometry.[10] Differently from tetrahedral and octahedral environments, where luminescence is associated to the $^4T_1(^4G)\rightarrow{}^6A_1(^6S)$ transition, in square-pyramidal complexes the transition involved is $^4E(^4G)\rightarrow{}^6A_1(^6S)$.

The examples provided highlight the rich coordination chemistry of Mn(II) with phosphine oxides, allowing the isolation of compounds with markedly different luminescence, depending *in primis* upon the coordination geometry. Another parameter to be considered is the presence of heavy atoms in the coordination sphere, causing an acceleration of the radiative decay because of an increased degree of spin–orbit coupling,[3] as previously observed for $[MnX_4]^{2-}$ compounds.[11] Phosphine

[a] *Dipartimento di Scienze Molecolari e Nanosistemi, Università Ca' Foscari Venezia, Via Torino 155, 30170 Mestre (VE), Italy. E-mail: markos@unive.it*
[b] *Consorzio Interuniversitario Reattività Chimica e Catalisi (CIRCC), via Celso Ulpiani 27, 70126 Bari, Italy*
[c] *Departamento de Química Inorgánica, Universidade de Vigo, Facultade de Química, Edificio de Ciencias Experimentais, 36310 Vigo, Galicia, Spain. E-mail: jesusc@uvigo.gal*
[d] *Dipartimento di Chimica e Chimica Industriale, Università di Pisa, Via G. Moruzzi 13, 56124 Pisa, Italy*

† Electronic Supplementary Information (ESI) available: superpositions of the $[MX_2L_2]$ complexes, Figures S1 and S2; parameters of selected planes in $[MnX_2L_2]$ complexes, Table S1; Cartesian coordinates of the DFT-optimized structures in .xyz format; CCDC 1999745, 1999746 and 1973290. For ESI and crystallographic data in CIF or other electronic format see DOI: 10.1039/x0xx00000x

oxides with suitable electronic structure can lead to the overlap of ligand-centred and metal-centred emissions, affording compounds with excitation-dependent luminescence.[8] Such a feature was recently reported also for Mn(II) complexes with N-donor ligands.[12] The peculiar emissive features suggest huge potential as inexpensive materials for advanced technology,[4] where $[MnX_4]^{2-}$ derivatives are already finding several applications.[13-16]

Besides phosphine oxides, phosphoramides represent another class of ligands suitable for the preparation of Mn(II) coordination compounds.[17-20] Tetrahedral green-emitting complexes were obtained using hexamethylphosphoramide as ligand. Its replacement in the coordination sphere with *N*,*N*,*N*′,*N*′-tetramethylphenylphosphonic diamide or 1,3-dimethyl-2-phenyl-1,3-diazaphospholidine-2-oxide highlighted the non-innocent role of the *P*-bonded phenyl substituent in Mn(II) luminescence sensitization.[21-22]

The increase of light harvesting by the coordinated [O=P]-donor ligands appears a suitable approach to enhance Mn(II) luminescence. In this communication we report the synthesis and characterization of three new tetrahedral complexes having general formula $[MnX_2L_2]$, where L is *N*,*N*,*N*′,*N*′-tetramethyl-*P*-indol-1-ylphosphonic diamide, containing a π-delocalized indolyl fragment.

Results and Discussion

Synthesis, characterization and X-ray structure determination of the complexes

The reaction of anhydrous MnX_2 salts (X = Cl, Br, I) with two equivalents of *N*,*N*,*N*′,*N*′-tetramethyl-*P*-indol-1-ylphosphonic diamide (L) in ethanol under mild conditions afforded complexes having general formula $[MnX_2L_2]$, as suggested by elemental analyses data. Conductivity measurements indicated the formation of neutral compounds. $^{31}P\{^1H\}$ NMR spectra revealed the absence of free ligand or diamagnetic phosphorous-containing species in the isolated products. The scarce differences in the IR spectra with respect to that of the free ligand are related to the weakening of the $\nu_{P=O}$ stretching attributable to coordination to Mn(II), as already observed for coordinated ligands based on the phosphoramide skeleton, and the consequent slight increase of the wavenumbers for to $\nu_{P\text{-}NMe2}$ stretching.[22-23] Figure 1 shows as an example the superposition of the IR spectra of L and $[MnBr_2L_2]$. The molar magnetic susceptibility values are in all the cases close to the ideal value for d^5 high spin first transition metal ions, this indicating negligible magnetic interactions among the Mn(II) centres.[24]

The formation of mononuclear complexes with tetrahedral geometry was confirmed by single-crystal X-ray diffraction. Figure 2 shows an ORTEP[25-26] representation of the compounds in different orientations. In the three complexes the manganese ion is coordinated by two halogen atoms and two oxygen atoms of the *N*,*N*,*N*′,*N*′-tetramethyl-*P*-indol-1-ylphosphonic diamide ligand.

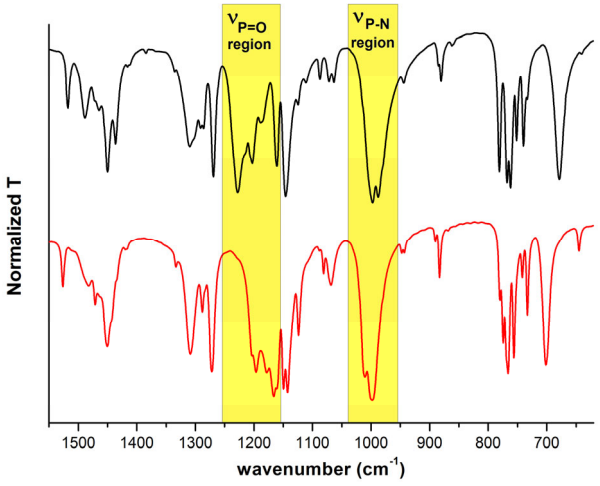

Fig. 1 Superposition of the IR spectra of L (black line) and $[MnBr_2L_2]$ (red line).

The three compounds are isomorphs, as demonstrated by Scheme 1, where a superimposition of the three molecules is sketched (carbon atoms in green, magenta and yellow for the chloro-, bromo- and iodo-complexes, respectively; similar schemes with superposition of couples of molecules are provided in ESI). In Table 1 the most significant distances and angles are set out, carefully ordered to show the small differences among them. The Mn-X bond lengths are in agreement with the change of the halogen, following the expected sequence Mn-Cl shorter than Mn-Br and this one shorter than Mn-I. The average Mn-O distances become shorter on increasing the Mn-X bond length. Other geometrical parameters in the diamide ligands are not influenced by the halogen. These features are in close agreement with those previously found in related compounds,[22] although it is worthy to mention that, to the best of our knowledge, only three compounds with the $[MnI_2(O{=}PR_3)_2]$ core were crystallografically described: $[MnI_2(O{=}PPh_3)_2]$ was studied thirty years ago;[27-28] the structure of $[MnI_2(O{=}PPh_2Me)_2]$ was also elucidated,[29] and more recently that of $[MnI_2(DPEPO)]$ (DPEPO = bis[2-(diphenylphosphino)phenyl] ether oxide).[3] The distortion of the coordination tetrahedron around the manganese atom in $[MnX_2L_2]$ can be described by the τ_4 parameter, 0.85 [X = Cl], 0.87 [X = Br] and 0.91 [X = I] (the extreme values are 0.00 for a square planar geometry and 1.00 for a perfect tetrahedron),[30] and by the dihedral angle between the MnX_2 and MnO_2 planes, 88.49(6) [X = Cl], 87.8(1) [X = Br] and 86.1(1)° [X = I]. Both the parameters let us to conclude a tetrahedral geometry around the Mn(II) centre, slightly distorted towards a seesaw. The angles around the manganese ion range from 104.72(4) to 116.111(12)° [extreme values for X = I]. X-Mn-X angle is always the most obtuse one, but in the $[MnX_2L_2]$ compounds the lower value corresponds to one of the X-Mn-O angles, O(1)-Mn-X(2), and not to the O-Mn-O one as in previous cases.[19-22] This anomalous situation reveals some distortion due the disposition of the ligands (see below).

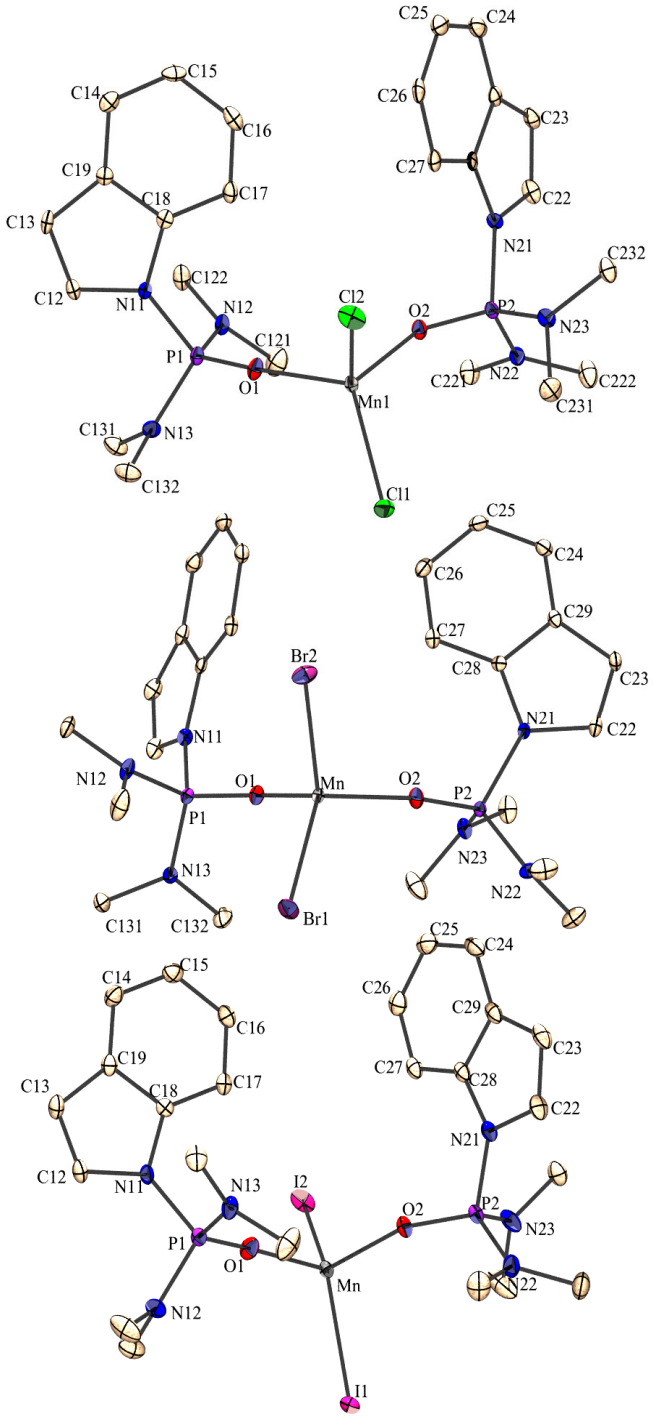

Fig. 2 ORTEP view of $[MnX_2L_2]$ (X = Cl, Br, I) compounds. Ellipsoids drawn at 50% probability level. Hydrogen atoms are not shown for clarity.

The P-O-Mn angles show another peculiarity, one of them is in the usual 145-150° range expected for this kind of $[MnX_2(O=PR_3)_2]$ complexes,[20-22] around 148.5° (see Table 1) but the other one is bigger, with values of 165.06(15) [X = Cl], 166.86(10) [X = Br] and 170.53(10)° [X = I]. These ones are only comparable with those found for a couple of iodo-complexes, 163.60(12)° in $[MnI_2(DPEPO)]$ [3] or 167.5° in $[MnI_2(O=PPh_2Me)_2]$.[29]

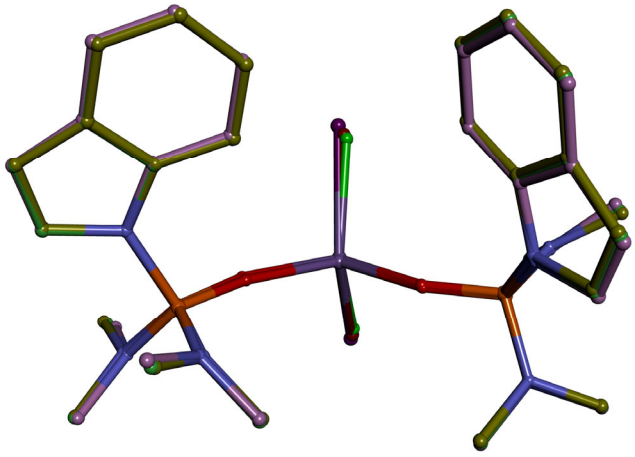

Scheme 1 Superimposition of the three $[MnX_2L_2]$ compounds.

Table 1. Selected bond lengths [Å] and angles [°] for $[MnX_2L_2]$.

	X=Cl	X=Br	X=I
Mn(1)-O(1)	2.045(2)	2.0328(14)	2.0237(14)
Mn(1)-O(2)	2.054(2)	2.0479(14)	2.0364(14)
Mn(1)-X(1)	2.3334(9)	2.4727(4)	2.6765(4)
Mn(1)-X(2)	2.3290(10)	2.4656(4)	2.6659(3)
P(1)-O(1)	1.485(2)	1.4884(14)	1.4861(14)
P(1)-N(11)	1.680(3)	1.6786(17)	1.6796(17)
P(1)-N(12)	1.621(3)	1.6230(17)	1.6235(17)
P(1)-N(13)	1.624(3)	1.6257(17)	1.6225(17)
P(2)-O(2)	1.492(2)	1.4912(14)	1.4950(14)
P(2)-N(21)	1.679(3)	1.6764(17)	1.6747(18)
P(2)-N(22)	1.620(3)	1.6230(17)	1.6197(18)
P(2)-N(23)	1.624(3)	1.6251(17)	1.6146(18)
O(1)-Mn(1)-O(2)	106.80(9)	106.75(6)	104.88(6)
X(1)-Mn(1)-X(2)	119.82(4)	118.433(13)	116.111(12)
O(1)-Mn(1)-X(1)	111.59(7)	111.94(4)	113.35(4)
O(2)-Mn(1)-X(1)	106.28(6)	106.54(4)	107.31(4)
O(1)-Mn(1)-X(2)	105.95(7)	105.60(4)	104.72(4)
O(2)-Mn(1)-X(2)	105.60(6)	106.96(4)	109.91(4)
P(1)-O(1)-Mn(1)	165.06(15)	166.86(10)	170.53(10)
P(2)-O(2)-Mn(1)	148.26(13)	148.43(9)	148.86(9)
O(1)-P(1)-N(11)	109.26(13)	109.12(9)	109.20(8)
O(1)-P(1)-N(12)	112.54(13)	111.17(9)	110.99(9)
O(1)-P(1)-N(13)	111.37(13)	112.47(9)	112.45(9)
N(11)-P(1)-N(12)	105.29(13)	107.47(9)	107.33(9)
N(12)-P(1)-N(13)	110.63(14)	110.65(9)	110.88(9)
N(11)-P(1)-N(13)	107.44(14)	105.67(9)	105.71(9)
O(2)-P(2)-N(21)	108.66(13)	108.45(8)	108.34(9)
O(2)-P(2)-N(22)	110.76(13)	114.59(9)	109.93(9)
O(2)-P(2)-N(23)	114.44(13)	110.29(9)	115.06(9)
N(21)-P(2)-N(22)	107.78(14)	104.44(9)	108.52(9)
N(22)-P(2)-N(23)	110.61(14)	110.57(9)	109.79(10)
N(21)-P(2)-N(23)	104.18(13)	108.12(9)	104.92(9)

We have previously found in the hexamethylphosphoramide (HMPA) compound $[MnBr_2\{O=P(NMe_2)_2\}_2]$ [20] that when three amides are bonded to a phosphorus atom, two of them are planar, but the third one shows some pyramidal shape. This situation was also found in $[MnX_2L_2]$ compounds, where the

indol-1-yl substituent has the role of one of the amides and exhibits pyramidal distortion on the nitrogen atom when the dimethylamides are planar. In this case, the P-O-Mn angle is almost linear. Otherwise, if the P-O-Mn angle is severely bent the indolyl nitrogen atom is planar, but the dimethylamide moieties are somewhat pyramidal (see Table S1 in ESI for more details).

Possible dispositions of the substituents around the phosphorus atoms are sketched in Scheme 2. The compounds described in this paper correspond to the third disposition. Noteworthy, $[MnBr_2\{O=PPh(NMe_2)_2\}_2]$ [20] showed two molecules in the asymmetric unit, corresponding to the first two dispositions in Scheme 2. Perhaps the intramolecular interaction C(27)-H(27)···X and the intermolecular ones reported in Table 2 favoured the third disposition in $[MnX_2L_2]$ derivatives.

The indol-1-yl moieties form a dihedral angle of 63.48(7) [X = Cl], 63.14(4) [X = Br] and 62.19(4)° [X = I] and this disposition allows a supramolecular framework mainly maintained by the intermolecular CH...X interactions set out in Table 2. As shown in Figure 3, each molecule acts as double H-donor interacting with two molecules, but it is also double H-acceptor by both iodine atoms, in such a way that each molecule is connected with other four ones. Figure 4 shows the holes found in the network, defined by the graph-set system [31] as $R_4^4(36)$. One molecule is connected with two neighbours, and both are connected with another one, to generate a 36-membered ring.

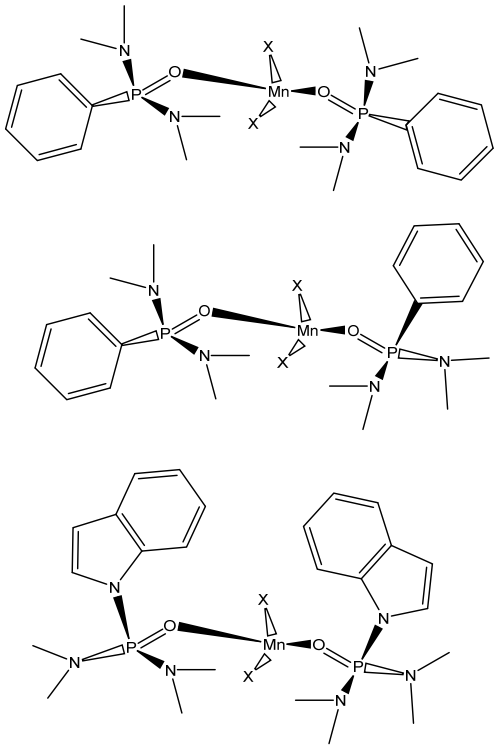

Scheme 2. Dispositions of the substituents around the phosphorus atoms in *N,N,N′,N′*-tetramethyl-*P*-phenyl-1-ylphosphonic diamide and *N,N,N′,N′*-tetramethyl-*P*-indol-1-ylphosphonic diamide derivatives.

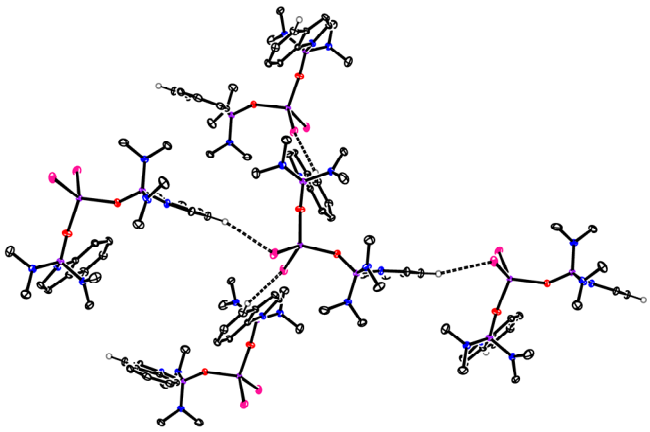

Fig. 3 $[MnI_2L_2]$ intermolecular interaction with four molecules.

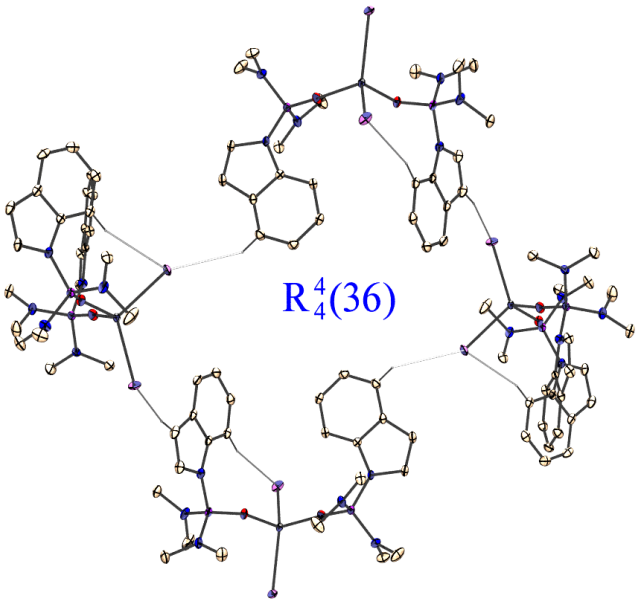

Fig. 4 36-membered ring formed by the interaction between four molecules, drawn for $[MnI_2L_2]$.

Table 2. Hydrogen bonds for the compounds. [Å and °].

D-H...A	d(D-H)	d(H...A)	d(D...A)	<(DHA)
$[MnCl_2L_2]$				
C(14)-H(14)...Cl(2^{i})	0.95	2.78	3.601(3)	145.8
C(23)-H(23)...Cl(1^{ii})	0.95	2.73	3.643(3)	161.7
C(27)-H(27)...Cl(2)	0.95	2.87	3.791(3)	165.0
Sym. Op.: i, 0.5-x, y+0.5, 0.5-z; ii, x-0.5, 0.5-y, z+0.5				
$[MnBr_2L_2]$				
C(14)-H(14)...Br(2^{i})	0.95	2.88	3.706(2)	146.5
C(23)-H(23)...Br(1^{ii})	0.95	2.82	3.742(2)	162.6
C(27)-H(27)...Br(2)	0.95	2.97	3.890(2)	163.4
Sym. Op.: i, 1.5-x, y-0.5, 1.5-z; ii, x+0.5, 1.5-y, z-0.5				
$[MnI_2L_2]$				
C(23)-H(23)...I(1^{i})	0.95	3.04	3.962(2)	165.5
C(14)-H(14)...I(2^{ii})	0.95	3.04	3.890(2)	149.9
C(27)-H(27)...I(2)	0.95	3.16	4.066(2)	160.3
Sym. Op.: i, x-0.5, 1.5-y, z+0.5; ii, 0.5-x, y-0.5, 0.5-z				

The compounds revealed to be moisture sensitive, but thermally stable, as deduced from DSC-TGA measurements. The DSC peaks corresponding to melting are comprised between 106 and 125°C. No meaningful mass loss occurs for temperatures below 230°C (see Figure 5).

Absorption and emission features

N,*N*,*N*′,*N*′-tetramethyl-*P*-indol-1-ylphosphonic diamide (L) was chosen as ligand to verify the possible enhancement of Mn(II) luminescence caused by the presence of a light harvesting substituent in the phosphoramide skeleton. The increased absorption in the UV range with respect to the related *N*,*N*,*N*′,*N*′-tetramethyl-*P*-phenylphosphonic diamide [21] is clearly observable from the superposition of the absorption spectra in Figure 6. The absorption (ABS) range is extended by about 20 nm and the integral area in the 235 – 300 nm range is five times greater for the indolyl derivative. The absorption features are unaltered by coordination to Mn(II) (see Table 3 and as an example the inset of Figure 6).

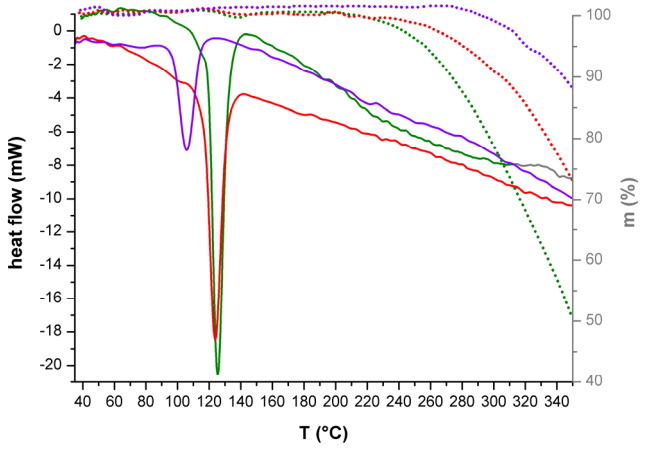

Fig. 5 DSC-TGA curves for $[MnX_2L_2]$ compounds. DSC, solid lines; TGA, dotted lines. X = Cl, green; X = Br, red; X = I, violet.

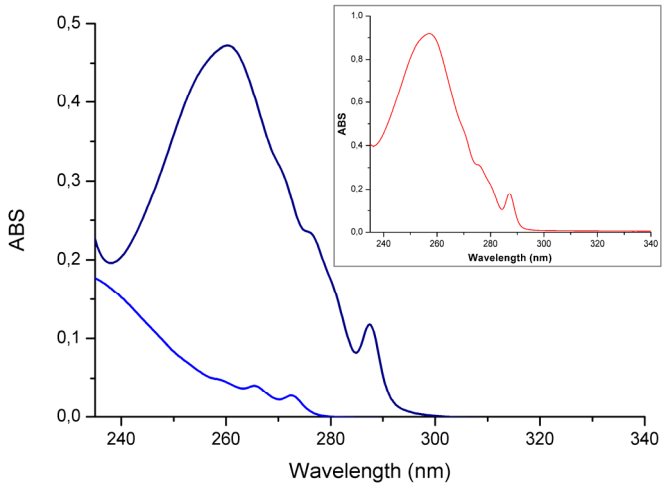

Fig. 6 Absorption spectra of *N*,*N*,*N*′,*N*′-tetramethyl-*P*-indol-1-ylphosphonic diamide (L, dark blue line) and *N*,*N*,*N*′,*N*′-tetramethyl-*P*-phenylphosphonic diamide (blue line). Inset: absorption spectrum of $[MnBr_2L_2]$. CH_2Cl_2 solution, $5 \cdot 10^{-5}$ M.

DFT calculations on the model system $[ZnCl_2L_2]$ confirmed that the absorptions are related to $\pi^* \leftarrow \pi$ transitions of the indolyl fragment. The superposition of occupied and unoccupied molecular orbitals involved in the lowest-energy absorption is shown as example in Figure 7. It is worth noting the involvement of the phosphorous atom in the unoccupied orbitals.

The solid $[MnX_2L_2]$ complexes are characterized by bright green emission upon excitation with UV light, quenched in solution. Normalized emission (PL) and excitation (PLE) spectra are collected in Figure 8 and data are summarized in Table 3. Powder and crystalline samples showed superimposable spectra. The PL bands are quite similar, centred between 519 and 535 nm and with FWHM values in the 2100 – 2800 cm^{-1} range, this suggesting comparable ligand field strengths. No shoulder attributable to the ground-state vibrational levels is present in the PL spectra. The chromaticity coordinated are shown in the CIE 1931 diagram reported in the inset of Figure 9. The emissions fall in the yellowish green region of the diagram (see Table 3), with colour purity around 80%. [32]

Accordingly to the literature, the PL bands are attributable to the Mn(II) $^4T_1(^4G) \rightarrow {}^6A_1(^6S)$ transition.[1-5] As observable in the inset of Figure 8, the excitation from the $^6A_1(^6S)$ ground state to the ^4G manifold falls in the violet-blue region of the visible spectrum.

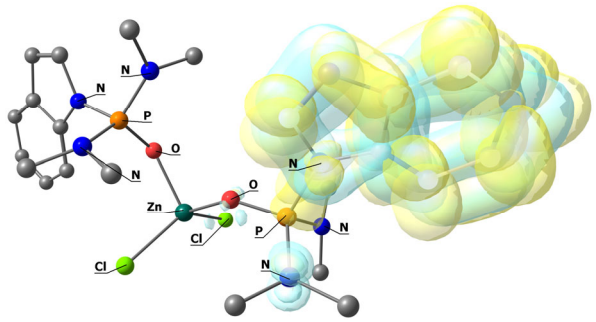

Fig. 7 Superposition of HOMO-1 and HOMO-3 orbitals (light blue tones) with LUMO and LUMO+2 orbitals (light yellow tones) of $[ZnCl_2L_2]$. Surface isovalue = 0.04 a.u. Carbon atoms in grey, hydrogen atoms omitted for clarity.

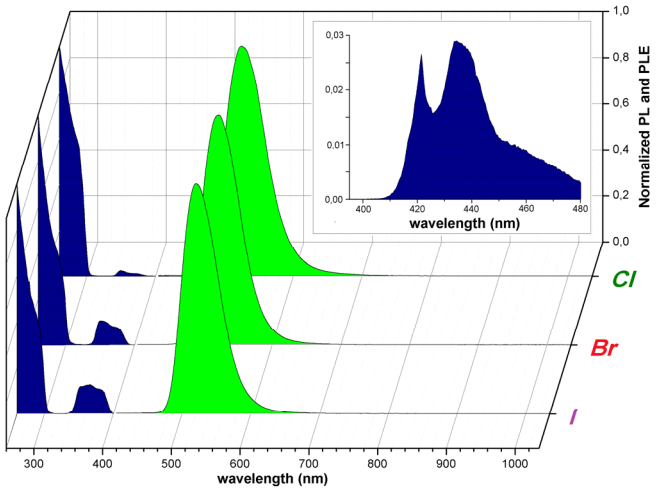

Fig. 8 Normalized PL and PLE spectra (UV range) of solid $[MnX_2L_2]$ complexes. Inset: PLE spectrum of $[MnCl_2L_2]$ in the visible region.

Table 3. Absorption and emission data of $[MnX_2L_2]$ complexes

X	ABS (nm)	PL (nm)	CIE	PLE	Lifetime (μs)
Cl	287, 276, 260 Ligands	527 $^4T_1(^4G)\rightarrow{}^6A_1(^6S)$ (FWHM = 2800 cm^{-1})	x = 0.287 y = 0.645	420-480 $^4G\leftarrow{}^6S$, 334-391 $^4P,^4D\leftarrow{}^6S$ < 315, 290 sh Ligands, $^4F\leftarrow{}^6S$	2198
Br	287, 276, 257 Ligands	535 $^4T_1(^4G)\rightarrow{}^6A_1(^6S)$ (FWHM = 2500 cm^{-1})	x = 0.255 y = 0.660	420-480 $^4G\leftarrow{}^6S$, 336-392 $^4P,^4D\leftarrow{}^6S$ < 315, 290 sh Ligands, $^4F\leftarrow{}^6S$	576
I	287, 275, 257 Ligands	519 $^4T_1(^4G)\rightarrow{}^6A_1(6S)$ (FWHM = 2100 cm^{-1})	x = 0.259 y = 0.665	420-480 ($^4G\leftarrow{}^6S$) , 336-392 ($^4P,^4D\leftarrow{}^6S$) < 315, 290 sh Ligands, $^4F\leftarrow{}^6S$	76

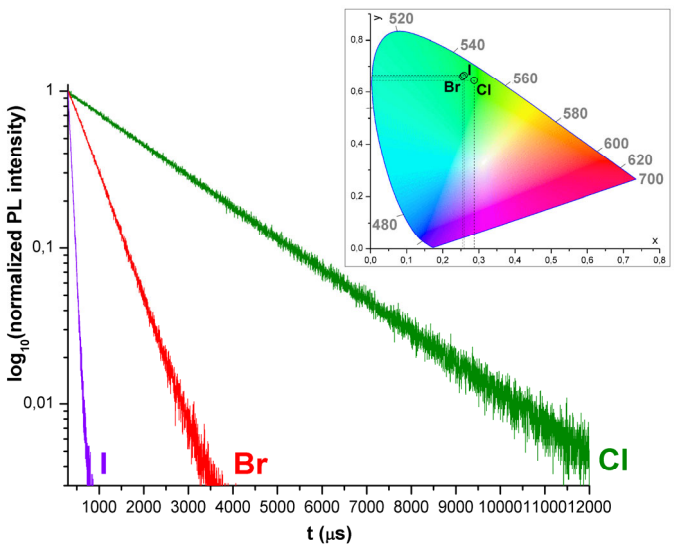

Fig. 9 Semi-log plot of luminescence decay curves. Inset: CIE 1931 chromaticity coordinates.

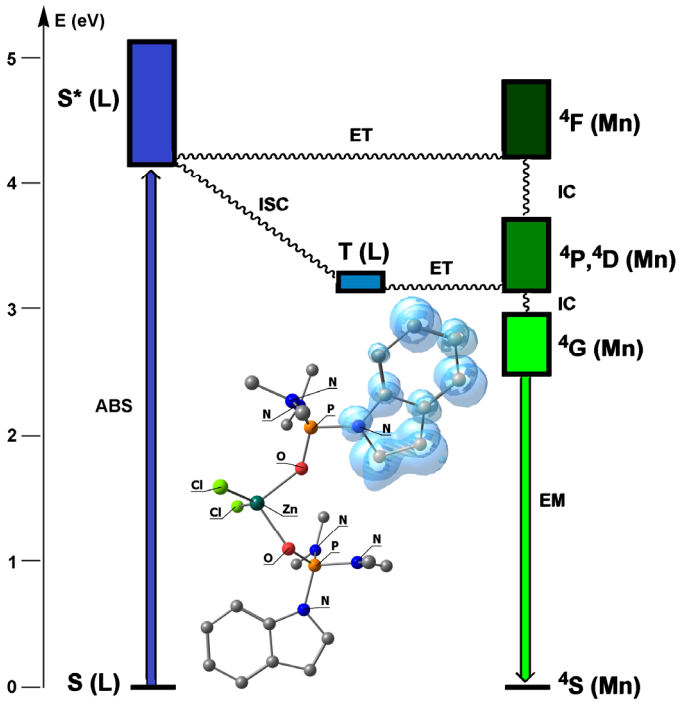

Fig. 10 Jablonski diagram for the $[MnX_2L_2]$ complexes and plot of the spin density of $[ZnCl_2L_2]$, triplet state. Surface isovalue = 0.005 a.u. Carbon atoms in grey, hydrogen atoms omitted for clarity.

Figure. 8 shows that the excitation in the UV-A range between 330 and 400 nm is attributable to Mn(II) transitions, the $^4P,^4D\leftarrow{}^6S$ in particular. On the other hand, excitation for wavelengths below 315 nm (UV-B,C) is mainly related to the energy transfer from the phosphoramide ligands to the excited states of the metal centre, superimposed to the $^4F\leftarrow{}^6S$ transitions.[21,33]. The emission spectra are not meaningfully influenced by the excitation wavelength, indicating that ligand-centred emissions do not compete with the ligand-to-metal energy transfer process. DFT calculations on $[ZnCl_2L_2]$ suggested that intersystem crossing following the ligands excitation is a possible intermediate step in the energy transfer towards Mn(II).[3] The relative energy of the $[ZnCl_2L_2]$ triplet state spans from 3.24 eV (singlet state geometry) to 3.16 eV (triplet state geometry), *i.e.* the 382 – 392 nm wavelength range, overlapping with the ^4D levels of tetrahedral Mn(II). The triplet state of the coordinated ligands is localized on the indol-1-yl fragment (see Figure 10). The absence of ligand-centred luminescence in $[MnX_2L_2]$ complexes can be explained on supposing that, after the triplet(L)$\rightarrow{}^4D$(Mn) energy transfer, fast internal conversion to the ^4G levels occurs. The proposed mechanism is depicted in the Jablonski diagram of Figure 10. The direct energy transfer from excited singlet states of the ligands to the energetically close Mn(II) ^4F manifold and the subsequent internal conversion cannot be however ruled out.

The nature of X affects the PLE spectra on changing the UV-A/UV-B,C excitation ratio, about 2% for the chloro-derivative, and 18% and 24% for the bromo- and iodo-complexes, respectively. Since UV-A PLE bands are exclusively related to direct Mn(II) excitation, their relative growth is attributable to increased spin-orbit coupling moving towards heavier halides, that causes the enhancement of Mn(II) direct absorption.[11]

Despite the fact that only qualitative comparisons can be done on solid samples, the emission intensity is clearly dependent upon the nature of the halide, also for excitation wavelengths involving the coordinated ligands. The intensity is comparable for $[MnBr_2L_2]$ and $[MnI_2L_2]$, but it is about 40% lower for $[MnCl_2L_2]$, as already observed for comparable species.[22] Because of the similar coordination sphere and the quite low wavenumbers of the Mn-X vibrations,[34] it is unlikely that such a variation could be related to non-radiative decay in the first coordination sphere. On the other hand, the higher spin-orbit coupling associated to the heavier halides could increase the

rates of intersystem crossing and ligand-to-metal energy transfer, thus reducing the influence of ligand-centred vibrational decays.

The influence of spin-orbit coupling is evident in the time-resolved photoluminescence spectra reported in Figure 9 (see also Table 3). The measured lifetime is around 2198 μs for the chloro-complex, much longer than that of the bromo-derivative, 576 μs. The value drops to 76 μs for $[MnI_2L_2]$. Such a trend is in line with previous reports on luminescent Mn(II) tetrahedral complexes.[22] The lifetime values are similar to those reported by Zheng *et al.* for $[MnX_2(DPEPO)]$ complexes.[3] The quantum yield measurements, limited to $[MnBr_2L_2]$ because of its better stability under air, gave an average value of 22%, close to that reported for $[MnBr_2(O=PPh_3)_2]$ [3] and comparable with related phenylphosphosphosphonic diamide complexes.[21-22]

Conclusions

N,*N*,*N'*,*N'*-tetramethyl-*P*-indol-1-ylphosphonic diamide represents a further step in the design of ligands different from phosphine oxides suitable for the sensitization of Mn(II) luminescence. It was confirmed that P-bonded aromatic substituents have a key role in the ligand-to-metal energy transfer, offering the possibility to overcome the limited direct Mn(II) excitation. Several further derivatizations of the phosphoramide skeleton can be proposed, and the low cost of the metal centre makes it of interest in the search of viable alternatives to low-abundant elements in optics and lighting technology.

Experimental section

Materials and methods

Commercial solvents (Aldrich) were purified as described in the literature.[35] Anhydrous Mn(II) halides were purchased from Alfa Aesar. The organic reactants were Aldrich products, used as received.

All the syntheses were carried out under inert atmosphere, working in a glove-box (MBraun Labstar with MB 10 G gas purifier) filled with N_2 and equipped for organic and inorganic syntheses.

N,*N*,*N'*,*N'*-tetramethyl-*P*-indol-1-ylphosphonic diamide (L) was synthesized on the basis of the methods reported in the literature.[36-37] Indole was deprotonated in THF with potassium *tert*-butoxide and then reacted with a stoichiometric amount of $O=P(NMe_2)_2Cl$ at room temperature in THF.

Elemental analyses (C, H, N) were carried out using an Elementar Unicube microanalyzer. Halide content was determined using the Mohr's method.[38] Magnetic susceptibilities were measured on solid samples at 298 K with a MK1 magnetic susceptibility balance (Sherwood Scientific Ltd) and corrected for diamagnetic contribution by means of tabulated Pascal's constants.[39] Melting points were registered employing a FALC 360 D instrument equipped with a camera. DSC-TGA measurements were carried out under N_2 atmosphere with a Linseis STA PT 1000 instrument. The heating rate was set at 10°C min^{-1}. Conductivity measurements were carried out using a Radiometer Copenhagen CDM83 instrument. IR spectra were collected in the range 4000 – 400 cm^{-1} using a Perkin-Elmer Spectrum One spectrophotometer. $^{31}P\{^1H\}$ NMR spectra were recorded with a Bruker Avance 400 instrument, using $CDCl_3$ as solvent.

Synthesis of $[MnX_2L_2]$ complexes (X = Cl, Br, I)

The complexes were isolated by slowly adding a solution containing 2.1 mmol (0.528 g) of L dissolved in 10 ml of EtOH into another solution of the proper anhydrous manganese salt MnX_2 (1 mmol) dissolved in 20 ml of EtOH. The reaction mixture was stirred overnight inside the glove-box at room temperature. The solvent was then evaporated under reduced pressure and the solid thus obtained was dissolved in the minimum amount of dichloromethane. The solution was cleared by centrifugation and the solvent was removed under reduced pressure. The product isolated by addition of diethyl ether was then filtered and dried *in vacuo*. Yield > 80% in all the cases. Crystals of $[MnCl_2L_2]$ and $[MnBr_2L_2]$ suitable for X-ray diffraction were obtained from slow evaporation of toluene/acetone solutions, while $[MnI_2L_2]$ was crystallized from dichloromethane/diethyl ether.

Characterization of $[MnCl_2L_2]$. Anal. calcd for $C_{24}H_{36}Cl_2MnN_6O_2P_2$ (628.37 g mol^{-1}, %): C, 45.87; H, 5.77; N, 13.37; Cl, 11.28. Found (%): C, 45.69; H, 5.79; N, 13.32; Cl, 11.32. M.p.: 122°C (DSC peak 125°C). χ_M^{corr} (c.g.s.u.): $1.48 \cdot 10^{-2}$. Λ_M (CH_2Cl_2, 298 K, Ohm^{-1} mol^{-1} cm^2): < 2. IR (cm^{-1}): 3150-3000 m/w (aromatic ν_{C-H}), 2980-2785 m (ν_{C-H}), 1550-1390 m (aromatic ν_{C-C} and ν_{C-N}), 1245-1095 s ($\nu_{P=O}$ and ν_{C-N}), 1040-920 s (ν_{P-N}).

Characterization of $[MnBr_2L_2]$. Anal. calcd for $C_{24}H_{36}Br_2MnN_6O_2P_2$ (717.28 g mol^{-1}, %): C, 40.19; H, 5.06; N, 11.72; Br, 22.28. Found (%): C, 40.03; H, 5.10; N, 11.77; Br, 22.19. M.p.: 120°C (DSC peak 124°C). χ_M^{corr} (c.g.s.u.): $1.47 \cdot 10^{-2}$. Λ_M (CH_2Cl_2, 298 K, Ohm^{-1} mol^{-1} cm^2): < 2. IR (cm^{-1}): 3150-3000 m/w (aromatic ν_{C-H}), 2980-2785 m (ν_{C-H}), 1550-1390 m (aromatic ν_{C-C} and ν_{C-N}), 1245-1095 s ($\nu_{P=O}$ and ν_{C-N}), 1040-920 s (ν_{P-N}).

Characterization of $[MnI_2L_2]$. Anal. calcd for $C_{24}H_{36}I_2MnN_6O_2P_2$ (811.28 g mol^{-1}, %): C, 35.53; H, 4.47; N, 10.36; I, 31.29. Found (%): C, 35.39; H, 4.50; N, 10.32; I, 31.42. M.p.: 99°C (DSC peak 106°C). χ_M^{corr} (c.g.s.u.): $1.49 \cdot 10^{-2}$. Λ_M (CH_2Cl_2, 298 K, Ohm^{-1} mol^{-1} cm^2): < 2. IR (cm^{-1}): 3150-3000 m/w (aromatic ν_{C-H}), 2980-2785 m (ν_{C-H}), 1550-1390 m (aromatic ν_{C-C} and ν_{C-N}), 1245-1095 s ($\nu_{P=O}$ and ν_{C-N}), 1040-920 s (ν_{P-N}).

Photoluminescence measurements

Absorption spectra in solution were collected using a Perkin-Elmer Lambda 35 spectrophotometer. Measurements on solid samples were carried out using air-tight quartz sample holders, filled in glove-box to avoid interactions of the complexes with moisture. Preliminary emission (PL) spectra were recorded in the range 400–1035 nm with an OceanOptics Flame-T spectrometer coupled with an optical fiber, a collimating lens and a

longpass filter, using UV led (280–375 nm) excitation sources. Photoluminescence emission (PL) and excitation (PLE) measurements were carried out at room temperature on solid samples by a Horiba Jobin Yvon Fluorolog-3 spectrofluorometer. A continuous-wave xenon arc lamp was used as source selecting the excitation wavelength by a double Czerny–Turner monochromator. A single grating monochromator coupled to a photomultiplier tube was used as detection system for optical emission measurements. Excitation and emission spectra were corrected for the instrumental functions. Time-resolved analyses were performed in multi channel scaling modality (MCS) by using a pulsed UV led source (Horiba SpectraLED, 290 nm). Decay curves were fitted with monoexponential functions.

Computational details

The computational geometry optimizations of the zinc complex in singlet and triplet states were carried out without symmetry constrains, using the range-separated hybrid functional ωB97X [40-42] and the def2 split-valence polarized basis set of Ahlrichs and Weigend.[43] The optimized electronic structures were then used for TD-DFT calculations.[44] The software used was Gaussian 09.[45]

Crystal structure determination

The crystallographic data were collected at CACTI (Universidade de Vigo) at 100 K (CryoStream 800) using a Bruker D8 Venture Photon 100 CMOS detector and Mo-Kα radiation (λ = 0.71073 Å) generated by an Incoatec high brilliance IμS microsource. The software APEX3 [46] was used for collecting frames of data, indexing reflections, and the determination of lattice parameters, SAINT [46] for integration of the intensity of reflections, and SADABS [46] for scaling and empirical absorption correction. The crystallographic treatment was performed using the Oscail program [47] and the structures were solved using the SHELXT program.[48] They were subsequently refined by a full-matrix least-squares based on F^2 using the SHELXL program.[49] Non-hydrogen atoms were refined with anisotropic displacement parameters. Hydrogen atoms were included in idealized positions and refined with isotropic displacement parameters. Further details concerning crystal data and structural refinement are given in Table 4. CCDC 1999745 (X = Cl), 1999746 (X = Br) and 1973290 (X = I) contain the supplementary crystallographic data for this paper.† PLATON (version 230318) [50] was used to obtain some geometrical parameters of the cif files.[51-55]

Table 4. Crystal data and structure refinement

Identification code	$[MnCl_2L_2]$	$[MnBr_2L_2]$	$[MnI_2L_2]$
Empirical formula	$C_{24}H_{36}Cl_2MnN_6O_2P_2$	$C_{24}H_{36}Br_2MnN_6O_2P_2$	$C_{24}H_{36}I_2MnN_6O_2P_2$
Formula weight	628.37	717.29	811.27
Temperature	100(2) K	100(2) K	100(2) K
Wavelength	0.71073 Å	0.71073 Å	0.71073 Å
Crystal system	Monoclinic	Monoclinic	Monoclinic
Space group	$P2_1/n$	$P2_1/n$	$P2_1/n$
Unit cell dimensions	a = 10.3500(8) Å	a = 10.4594(5) Å	a = 10.6662(7) Å
	b = 15.7450(13) Å	b = 15.7962(8) Å	b = 15.8451(12) Å
	c = 18.6481(14) Å	c = 19.0025(9) Å	c = 19.6427(15) Å
	β = 99.437(2)°	β = 99.319(2)°	β = 100.640(2)°
Volume	2997.8(4) Å^3	3098.1(3) Å^3	3262.7(4) Å^3
Z	4	4	4
Density (calculated)	1.392 Mg/m^3	1.538 Mg/m^3	1.652 Mg/m^3
Absorption coefficient	0.758 mm^{-1}	3.140 mm^{-1}	2.425 mm^{-1}
F(000)	1308	1452	1596
Crystal size	0.172 x 0.109 x 0.047 mm	0.263 x 0.259 x 0.121 mm	0.235 x 0.226 x 0.169 mm
Θ range for data collection	2.214 to 26.456°	2.357 to 28.368°	2.330 to 28.377°
Index ranges	$-12 \le h \le 12$	$-13 \le h \le 13$	$-14 \le h \le 12$
	$-19 \le k \le 19$	$-21 \le k \le 20$	$-20 \le k \le 21$
	$-19 \le l \le 23$	$-24 \le l \le 25$	$-25 \le l \le 26$
Reflections collected	25091	69466	56685
Independent reflections	6164 [R_{int} = 0.0908]	7731 [R_{int} = 0.0606]	8153 [R_{int} = 0.0373]
Reflections observed (>2σ)	4240	6776	7437
Data Completeness	0.995	0.999	0.998
Absorption correction	Semi-empirical from equivalents	Semi-empirical from equivalents	Semi-empirical from equivalents
Max. and min. transmission	0.7425 and 0.6431	0.7457 and 0.3403	0.7457 and 0.5669
Refinement method	Full-matrix least-squares on F^2	Full-matrix least-squares on F^2	Full-matrix least-squares on F^2
Data / restraints / parameters	6164 / 0 / 342	7731 / 0 / 342	8153 / 0 / 342
Goodness-of-fit on F^2	1.010	1.055	1.090
Final R indices [$I>2\sigma(I)$]	R_1 = 0.0514	R_1 = 0.0302	R_1 = 0.0234
	wR_2 = 0.0840	wR_2 = 0.0655	wR_2 = 0.0509
R indices (all data)	R_1 = 0.0974	R_1 = 0.0380	R_1 = 0.0280
	wR_2 = 0.0959	wR_2 = 0.0680	wR_2 = 0.0522
Largest diff. peak and hole	0.390 and -0.425 e.Å-3	0.448 and -0.747 e.Å-3	0.742 and -1.000 e.Å-3

Conflicts of interest

There are no conflicts to declare.

Acknowledgements

Università Ca' Foscari Venezia is gratefully acknowledged for financial support (Bando Progetti di Ateneo 2014, D. R. 553/2014 prot. 31352; Bando Spin 2018, D. R. 1065/2018 prot. 67416). CACTI (University of Vigo) is gratefully acknowledged for X-ray data collection.

Notes and references

1 D. M. L. Goodgame and F. A. Cotton, *J. Chem. Soc.*, 1961, 3735–3741, DOI: 10.1039/JR9610003735.
2 Y.-Y. Tang, Z.-X. Wang, P.-F. Li, Y.-M. You, A. Stroppa and R.-G. Xiong, *Inorg. Chem. Front.*, 2017, **4**, 154–159, DOI: 10.1039/c6qi00148c.
3 J. Chen, Q. Zhang, F.-K. Zheng, Z.-F. Liu, S.-H. Wang, A.-Q. Wu and G.-C. Guo, *Dalton Trans.*, 2015, **44**, 3289–3294, DOI: 10.1039/C4DT03694H.
4 Y. Y. Qin, P. Tao, L. Gao, P. F. She, S. J. Liu, X. L. Li, F. Y. Li, H. Wang, Q. Zhao, Y. Q. Miao and W. Huang, *Adv. Opt. Mater.*, 2019, **7**, 1801160, DOI: 10.1002/adom.201801160
5 Y. Wu, X. Zhang, L.-J. Xu, M. Yang and Z.-N. Chen, *Inorg. Chem.*, 2018, **57**, 9175–9181, DOI: 10.1021/acs.inorgchem.8b01205.
6 M. Bortoluzzi, J. Castro, E. Trave, D. Dallan and S. Favaretto, *Inorg. Chem. Commun.*, 2018, **90**, 105–107, DOI: 10.1016/j.inoche.2018.02.018.
7 A. S. Berezin, D. G. Samsonenko, V. K. Brelc and A V. Artem'ev, *Dalton Trans.* 47 (2018) 7306–7315, DOI: 10.1039/c8dt01041b.
8 M. P. Davydova, I. A. Bauer, V. K. Brel, M. I. Rakhmanova, I. Yu. Bagryanskaya and A. V. Artem'ev, *Eur. J. Inorg. Chem.*, 2020, 695–703, DOI: 10.1002/ejic.201901213.
9 A. S. Berezin, M. P. Davydova, I. Yu. Bagryanskaya, O. I. Artyushin, V. K. Brel and A. V. Artem'ev, *Inorg. Chem. Commun.*, 2019, **107**, 107473, DOI: 10.1016/j.inoche.2019.107473.
10 A. V. Artem'ev, M. P. Davydova, A. S. Berezin, V. K. Brel, V. P. Morgalyuk, I. Yu. Bagryanskaya and D. G. Samsonenko, *Dalton Trans*. 2019, **48**, 16448–16456, DOI: 10.1039/c9dt03283e.
11 M. Wrighton and D. Ginley, *Chem. Phys.*, 1974, **4**, 295–299, DOI: 10.1016/0301-0104(74)80097-2.
12 A. S. Berezin, K. A. Vinogradova, V. A. Nadolinny, T. S. Sukhikh, V. P. Krivopalov, E. B. Nikolaenkova and M. B. Bushuev, *Dalton Trans.*, 2018, **47**, 1657–1665, DOI: 10.1039/c7dt04535b.
13 L.-J. Xu, C.-Z. Sun, H. Xiao, Y. Wu and Z.-N. Chen, *Adv. Mater.*, 2017, **29**, 1605739, DOI: 10.1002/adma.201605739.
14 S. Chen, J. Gao, J. Chang, Y. Zhang and L. Feng, *Sens. Actuators B*, 2019, **297**, 126701, DOI: 10.1016/j.snb.2019.126701.
15 C. Jiang, N. Zhong, C. Luo, H. Lin, Y. Zhang, H. Peng and C.-G. Duan, *Chem. Commun.*, 2017, **53**, 5954–5957, DOI: 10.1039/C7CC01107E.
16 S. Balsamy, P. Natarajan, R. Vedalakshmi and S. Muralidharan, *Inorg. Chem.*, 2014, **53**, 6054–6059, DOI: 10.1021/ic500400y.
17 Y. Abe and G. Wada, *Bull. Chem. Soc. Jpn.*, 1980, **53**, 3547–3551, DOI: 10.1246/bcsj.53.3547.
18 Y. Abe and G. Wada, *Bull. Chem. Soc. Jpn.*, 1981, **54**, 3334–3339, DOI: 10.1246/bcsj.54.3334.
19 Z. M. Jin, B. Tu, Y. Q. Li and M. C. Li, *Acta Crystallogr. Sect. E*, 2005, **61**, m2510–m2511, DOI: 10.1107/S1600536805035506
20 M. Bortoluzzi and J. Castro, *J. Coord. Chem.*, 2019, **72**, 309–327, DOI: 10.1080/00958972.2018.1560430.
21 M. Bortoluzzi, J. Castro, F. Enrichi, A. Vomiero, M. Busato and W. Huang, *Inorg. Chem. Commun.*, 2018, 92, 145–150, DOI: 10.1016/j.inoche.2018.04.023.
22 M. Bortoluzzi, J. Castro, A. Gobbo, V. Ferraro, L. Pietrobon and S. Antoniutti, *New J. Chem.* 2020, **44**, 571–579, DOI: 10.1039/c9nj05083c.
23 S. P. Sinha, T. T. Pakkanen, T. A. Pakkanen and L. Niinistö, *Polyhedron*, 1982, **1**, 355–359, DOI: 10.1016/S0277-5387(00)80819-0.
24 R. S. Nyholm, *J. Inorg. Nucl. Chem.*, 1958, **8**, 401–422, DOI: 10.1016/0022-1902(58)80206-7.
25 L. J. Farrugia, *J. Appl. Crystallogr.*, 1997, **30**, 565, DOI: 10.1107/S0021889897003117.
26 *POV-Ray v3.7 for Windows, Persistence of Vision Raytracer*, Persistence of Vision Pty. Ltd., 2016, http://www.povray.org/documentation.
27 B. Beagley, C. A. McAuliffe, R. G. Pritchard and E. W. White, *Acta Chem. Scand.*, 1988, **42,** 544–553, DOI: 10.3891/acta.chem.scand.42a-0544.
28 T. Avilés, M. A. A. F. de C. T. Carrondo, M. F. M. Piedade and G. Teixeira, *J. Organomet. Chem*., 1990, **388**, 143–149, DOI: 10.1016/0022-328X(90)85356-4.
29 S. M. Godfrey, C. A. McAuliffe, P. T. Ndifon and R. G. Pritchard, *J. Chem. Soc., Dalton Trans.,* 1993**,** 3373–3377, DOI: 10.1039/dt9930003373.
30 L. Yang, D. R. Powell and R. P. Houser, *Dalton Trans*. 2007, 955–964, DOI: 10.1039/B617136B.
31 J. Grell, J. Bernstein and G. Tinhofer, *Acta Crystallogr*. 1999, **B55**, 1030–1043, DOI: 10.1107/S0108768199015967.
32 E. F. Schubert, *Light-emitting Diodes*, Cambridge University Press, 2nd edn, 2006, pp. 292–300.
33 F. A. Cotton, D. M. L. Goodgame and M. Goodgame, *J. Am. Chem. Soc.*, 1962, **84**, 167–172, DOI: 10.1021/ja00861a008.
34 H. G. M. Edwards, M. J. Ware and L. A. Woodward, *Chem. Commun. (London)*, 1968, 540-541, DOI: 10.1039/C19680000540.
35 W. L. F. Armarego and D. D. Perrin, *Purification of laboratory chemicals*, Butterworth-Heinemann, Oxford, 4th edn, 1996.
36 B. G. Van den Bos, C. J. Schoot, M. J. Koopmans and J. Meltzer, *Recl. Trav. Chim. Pay-B*, 1961, **80**, 1040–1047, DOI: 10.1002/recl.19610800913.
37 M. Bortoluzzi, A. Gobbo, A. Palù, F. Enrichi and A. Vomiero, *Chem. Pap.*, 2020, DOI: 10.1007/s11696-019-00799-6.
38 D. J. Pietrzyk and C. W. Frank, *Analytical Chemistry*, Academic Press, New York, 2nd edn, 2012.
39 G. A. Bain and J. F. Berry, *J. Chem. Ed.*, 2008, **85**, 532–536, DOI: 10.1021/ed085p532.
40 Y. Minenkov, Å. Singstad, G. Occhipinti and V. R. Jensen, *Dalton Trans.*, 2012, **41**, 5526–5541, DOI: 10.1039/c2dt12232d.
41 J.-D. Chai and M. Head-Gordon, *Phys. Chem. Chem. Phys.*, 2008, **10**, 6615–6620, DOI: 10.1039/b810189b.
42 I. C. Gerber and J. G. Ángyán, *Chem. Phys. Lett.*, 2005, **415**, 100–105, DOI: 10.1016/j.cplett.2005.08.060.
43 F. Weigend and R. Ahlrichs, *Phys. Chem. Chem. Phys.*, 2005, **7**, 3297–3305, DOI: 10.1039/b508541a.
44 C. A. Ullrich, *Time-Dependent Density Functional Theory*, Oxford University Press, Oxford, 2012.
45 M. J. Frisch, G. W. Trucks, H. B. Schlegel, G. E. Scuseria, M. A. Robb, J. R. Cheeseman, G. Scalmani, V. Barone, B. Mennucci, G. A. Petersson, H. Nakatsuji, M. Caricato, X. Li, H. P.

Hratchian, A. F. Izmaylov, J. Bloino, G. Zheng, J. L. Sonnenberg, M. Hada, M. Ehara, K. Toyota, R. Fukuda, J. Hasegawa, M. Ishida, T. Nakajima, Y. Honda, O. Kitao, H. Nakai, T. Vreven, J. A. Montgomery Jr., J. E. Peralta, F. Ogliaro, M. Bearpark, J. J. Heyd, E. Brothers, K. N. Kudin, V. N. Staroverov, R. Kobayashi, J. Normand, K. Raghavachari, A. Rendell, J. C. Burant, S. S. Iyengar, J. Tomasi, M. Cossi, N. Rega, J. M. Millam, M. Klene, J. E. Knox, J. B. Cross, V. Bakken, C. Adamo, J. Jaramillo, R. Gomperts, R. E. Stratmann, O. Yazyev, A. J. Austin, R. Cammi, C. Pomelli, J. W. Ochterski, R. L. Martin, K. Morokuma, V. G. Zakrzewski, G. A. Voth, P. Salvador, J. J. Dannenberg, S. Dapprich, A. D. Daniels, Ö. Farkas, J. B. Foresman, J. V. Ortiz, J. Cioslowski and D. J. Fox, *Gaussian 09, Revision C.01*, Gaussian Inc, Wallingford CT, 2010.

46 *Bruker*, *APEX3*, *SMART*, *SAINT*, Bruker AXS Inc., Madison, Wisconsin, USA, 2015.

47 P. McArdle, K. Gilligan, D. Cunningham, R. Dark and M. Mahon, *CrystEngComm*, 2004, **6**, 303–309, DOI: 10.1039/b407861f.

48 G. M. Sheldrick, *Acta Crystallogr., Sect. A: Found. Crystallogr.*, 2015, **A71**, 3–8, DOI: 10.1107/S2053273314026370.

49 G. M. Sheldrick, *Acta Crystallogr., Sect. C: Struct. Chem.*, 2015, **71**, 3–8, DOI: 10.1107/S2053229614024218.

50 A. L. Spek, *Acta Crystallogr., Sect. D: Biol. Crystallogr.*, 2009, **D65**, 148–155, DOI: 10.1107/S090744490804362X.

51 S. J. Grabowski, *Crystals*, 2016, **6**, 59, DOI: 10.3390/cryst6050059.

52 S. J. Grabowski, *Chem. Rev.*, 2011, **111**, 2597–2625, DOI: 10.1021/cr800346f.

53 R. Taylor, *Cryst. Growth Des.*, 2016, **16**, 4165–4168, DOI: 10.1021/acs.cgd.6b00736.

54 R. Taylor, *CrystEngComm*, 2014, **16**, 6852–6865, DOI: 10.1039/c4ce00452c.

55 T. Steiner, *Angew. Chem., Int. Ed.*, 2002, **41**, 48–76, DOI: 10.1002/1521-3773(20020104)41:1<48::AID-ANIE48>3.0.CO;2-U.